ACS APPLIED MATERIALS & INTERFACES

Research Article

www.acsami.org

# BMP7-Based Functionalized Self-Assembling Peptides for Nucleus Pulposus Tissue Engineering

Hui Tao,[†,‡,⊥] Yaohong Wu,[§,⊥] Haifeng Li,[†,⊥] Chaofeng Wang,[†] Yan Zhang,[†] Chao Li,[†] Tianyong Wen,[†] Xiumei Wang,[∥] Qing He,[†] Deli Wang,[*,†] and Dike Ruan[*,†]

[†]Department of Orthopaedic Surgery, Navy General Hospital, Beijing 100037, People's Republic of China

[‡]Department of Orthopaedic Surgery, The First Affiliated Hospital of Anhui Medical University, Hefei, Anhui 230031, People's Republic of China

[§]The Third Affiliated Hospital of Southern Medical University, Guangzhou 510665, People's Republic of China

[∥]State Key Laboratory of New Ceramics and Fine Processing, School of Materials Science and Engineering, Tsinghua University, Beijing 100084, People's Republic of China

**ABSTRACT:** Nucleus pulposus (NP) tissue engineering has been demonstrated to be a feasible therapeutic strategy for intervertebral disc regeneration. In this study, we constructed a novel injectable biomaterial by conjugating three different short peptides of BMP7 to the C-terminus of the self-assembling peptide RADA16-I, and we then mixed each of these conjugates with RADA16-I at equal volumes to obtain the novel functionalized peptides RAD-SNV, RAD-KPS, and RAD-KAI. The bioactivities of these functionalized peptides for human degenerated NP cells (hdNPCs) were evaluated in vitro, and the most ideal scaffold was chosen for assessment of its in vivo degradation and the tissue reactions to it. All of the functionalized peptides self-assembled to form hydrogel scaffolds with a nanofibrous structure under physiological conditions. Compared with the RADA16-I and RAD-KAI scaffolds, the RAD-SNV and RAD-KPS scaffolds possessed better bioactivities for hdNPCs, which were characterized by their enhanced proliferation, migration, and ECM (collagen II, aggrecan, and sox-9) secretion. RAD-KPS was chosen over RAD-SNV as the most ideal scaffold material due to the cells' higher rate of expression of aggrecan both at the gene and protein level after 28 days of coculture. Moreover, in vivo analysis demonstrated that subcutaneously injected RAD-KPS degraded in vivo without invoking intense inflammation. Therefore, RAD-KPS is an ideal candidate scaffold for NP tissue engineering and holds great potential for NP regeneration.

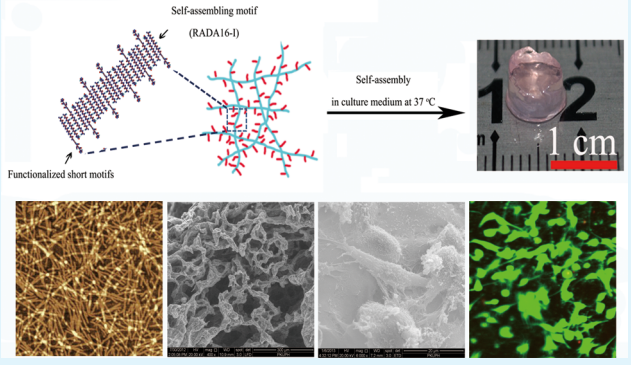


**KEYWORDS:** *intervertebral disc, degeneration, functional peptide, self-assembly, hydrogel, compatibility*

## 1. INTRODUCTION

Low back pain (LBP) is a major cause of disability throughout the world, with an estimated 70% to 80% of the population predicted to experience LBP at some point in their lives.[1] As the global population ages, the incidence of LBP increases. This condition imposes an enormous socio-economic burden on countries due to its effects on healthcare expenditures and loss of work. In the U.S.A. alone, it was estimated that the cost of LBP, which included direct and indirect lost productivity and disability benefit costs, was approximately $100 billion annually.[2] Although the causes of LBP are multifactorial, increasing evidence has implicated intervertebral disc degeneration (IDD) as a major contributor.[3,4] Current clinical therapies for IDD typically begin with nonoperative treatments, including physiotherapy or pain medication.[5−7] Surgical remedies, such as disc decompression or fusion or disc arthroplasty, are employed as the last resort and may cause many complications, such as adjacent segment degeneration and the loss of spinal mobility.[8−10] However, all of the above treatments relieve only the symptoms and were usually used for the patients with severe IDD. These treatments neither arrest the progression of IDD nor reverse IDD, particularly when they are provided during the early stage of IDD.

Although the exact pathogenesis of IDD remains unclear, IDD is widely attributed to the degeneration of the nucleus pulposus (NP).[11] With NP degeneration, there is a shift in the homeostatic balance between anabolism and catabolism, resulting in a decreased level of secretion of extracellular matrix (ECM) components, particularly aggrecan and collagen II$\alpha$1.[12] Aggrecan is the most abundant proteoglycan in the NP and is essential to maintaining its water content.[13] As a result of the decreased level of aggrecan, decreased hydrostatic pressure and the loss of disc height occur, which leads to further vertebral instability,

**Received:** April 26, 2015
**Accepted:** July 21, 2015
**Published:** July 21, 2015





DOI: 10.1021/acsami.5b03605
*ACS Appl. Mater. Interfaces* 2015, 7, 17076−17087

inflammatory changes, and disk herniation, resulting in back pain.[14] Therefore, one goal of IDD therapies must be to increase the secretion of ECM components in the NP, particularly that of aggrecan.

In light of this consideration, many biological therapeutic strategies for the treatment of IDD have been explored, and tremendous progress has been made in the past decade.[15] Among such strategies, the most common are injecting growth factors, cell transplantation, and the implantation of hydrogel-based medical devices.[16−21] It has been confirmed that these treatments not only showed promising results in vitro, such as stimulating the proliferation of NP cells and/or elevating the aggrecan content of the NP, but these treatments have also exhibited regenerative potential in vivo, involving improving the water content level and/or restoring the height of degenerated intervertebral discs. However, a number of problems remain to be solved, including the short-lived effect of growth-factor injection and the identification of suitable biomaterials. Thus, emphasis has shifted toward biomaterials with which growth factors could be incorporated for the biological treatment of IDD with long-term efficacy.

Recently, self-assembling peptide scaffolds have become a topic of intensive biomaterial research.[22] Unlike other biomaterials, such as collagen, laminin, and Matrigel, which carry the risk of chemical and biological contaminants due to their origin (being chemosynthesized or isolated from living tissues), self-assembling peptide scaffolds are produced using natural amino acids, which could reduce the risk of the above-mentioned problems. Furthermore, self-assembling peptides can undergo self-assembly to form nanofibrous hydrogel scaffolds under physiological conditions, and these scaffolds consisted of >99% water, with fibers of ∼10 nm in diameter and pores of 5−200 nm in size, making their structures very similar to that of a natural extracellular matrix (ECM).[23] These nanofibrous hydrogel scaffolds have been demonstrated to be unique biomaterials with various applications, including in three-dimensional (3D) cell culture, tissue engineering, regenerative medicine, and drug release.[24−36] RADA16-I (Ac-RADARADARADARA DA-$CONH_2$) is a very important member of the self-assembling peptide family. RADA16-I consists of 16-residue peptides, which can undergo molecular self-assembly to form nanofibers by creating stable $\beta$-sheet structures within water.[26] The nanofibers then form higher-order interwoven nanofibrous hydrogel scaffolds under physiological conditions via alternating hydrophobic and hydrophilic amino acids.[23] In addition, one of the most important features of RADA16-I is that various bioactive short-peptide motifs can be easily conjugated to its C-terminus to produce analogues of growth factors. A number of functionalized RADA16-I hydrogels have been designed and tested for their biological applications, including in bone, neural, myocardial, and angiogenic regeneration.[27−30] These studies demonstrated that functionalized self-assembling RADA16-I peptides exhibited the potential for promising applications in tissue regeneration.

Previous studies demonstrated that bone morphogenetic protein-7 (BMP7, also called osteogenic protein-1) had a very important effect on a degenerated disc.[31,32] BMP7 not only stimulated nucleus pulposus cells to secrete aggrecan and collagen II in vitro but also prevented disc degeneration in vivo.[31,33] Moreover, Chen et al.[34] showed that three different short peptides (SNVILKKYRN [SNV], KPSSAPTQLN [KPS], and KAISVLYFDDS [KAI]) of BMP7 displayed its master functionalities. In our previous study,[35] we successful conjugated one important short peptide, KPS, to the C-terminus of RADA16-I to obtain a novel functionalized self-assembling peptide RKP and found that it could be used to form excellent scaffolds for NP tissue engineering when mixed with RADA16-I at an equal volume ratio. However, BMP7 contains three different important short functional motifs, as above-mentioned. Which one is optimal for use as a C-terminal conjugate of RADA16-I in NP tissue engineering is unknown.

Therefore, in this study, we first conjugated SNV, KPS, and KAI to the C-terminus of RADA16-I to obtain three different peptides. Second, these peptides were mixed with RADA16-I to form three novel functionalized self-assembling peptides RAD-SNV, RAD-KPS and RAD-KAI. Finally, the biocompatibilities and bioactivities of these three different functionalized self-assembling peptides with human degenerated nucleus pulposus cells (hdNPCs) were assessed in vitro, and the optimal molecule was chosen for in vivo evaluation of its biocompatibility.

## 2. MATERIALS AND METHODS

**2.1. Synthesis of the Designer Self-Assembling Peptides and Scaffold Preparation.** All the peptides used in this work were custom-synthesized at Sangon Biotech (purity >90%, Shanghai, China). The peptide sequences are listed in Table 1. These peptide powders were dissolved in distilled water at a final concentration of 1% (w/v, 10 mg/mL), using 30 min of sonication. All of the peptide solutions were filter-sterilized using syringe-driven filter units (0.22-$\mu$m HT Tuffryn membrane, Pall Corp., Ann Arbor, MI, U.S.A.) prior to their use. Each of the designer functionalized peptide solutions was mixed with a solution of 1% pure RADA16-I in a volume ratio of 1:1 to obtain the 1% functionalized peptide mixtures (RAD-SNV, RAD-KPS, and RAD-KAI).

**Table 1. Peptide Sequences of the Designer Self-Assembling Peptides**

| name | sequences |
|---|---|
| RADA16-I | AC-RADARADARADARADA-$CONH_2$ |
| SNV | AC-$(RADA)_4$-GG-SNVILKKYRN-$CONH_2$ |
| KPS | AC-$(RADA)_4$-GG-KPSSAPTQLN-$CONH_2$ |
| KAI | AC-$(RADA)_4$-GG-KAISVLYFDDS-$CONH_2$ |

Cell culture transwell inserts (6.5 mm diameter, 0.4-$\mu$m pore polyester membrane) were used for the preparation of the self-assembling peptide hydrogels, as previously described. Briefly, the insets were placed in a 24-well culture plate, and 400 $\mu$L of basal culture medium (Dulbecco's modified Eagle's medium and Ham's F12 medium, DMEM/F12, Hyclone) was added to each well. Then, 100 $\mu$L of a peptide solution (RADA16-I, RAD-SNV, RAD-KPS or RAD-KAI) was added, and the plate was incubated at 37 °C for 1 h to allow gelation to occur. Subsequently, 400 $\mu$L of culture medium was gently loaded onto the gel and the plate was then incubated overnight at 37 °C in 5% $CO_2$. Before the hydrogel scaffolds were used, the medium was carefully removed and then was changed twice to wash away any free acid residues remaining from peptide synthesis. Then, the medium was changed every 2 days.

**2.2. Atomic-Force Microscopy (AFM) Assessment of Self-Assembling Peptides.** All of the peptide solutions (RADA16-I, RAD-SNV, RAD-RPS, and RAD-KAI) were diluted to a working concentration of 0.01% (w/v). Five microliters of each diluted sample was dropped onto a freshly cleaved mica surface and left for 5 s, and then the surface was gently rinsed twice using 100 $\mu$L of distilled water. The peptide samples on the


DOI: 10.1021/acsami.5b03605
ACS Appl. Mater. Interfaces 2015, 7, 17076−17087

mica surface were then air-dried at room temperature for 3−4 h. Images of the samples were acquired using an AFM (SPA-300 HV, Seiko Instruments, Japan). The scanning area was 1 × 1 $\mu$m, and the frequency was 1.02 Hz.

**2.3. Circular Dichroism (CD) Assessment of Self-Assembling Peptides.** All of the peptide samples were prepared by diluting 1% peptide solutions in distilled water to a working concentration of 50 $\mu$M. Then, the samples were incubated at room temperature overnight. The CD spectra were collected using a quartz curet with a path length of 0.5 cm, in a wavelength range of 195−250 nm. Each spectrum was collected in triplicate.

**2.4. Rheological Analysis of Self-Assembling Peptides.** The rheological behavior of the peptide samples was evaluated using a RheoStress AR G2 instrument (TA Instruments, Inc., U.S.A.). One milliliter of each 1% (w/v) peptide solution (RADA16-I, RAD-SNV, RAD-KPS, and RAD-KAI) was mixed with 500 $\mu$L of DMEM at a ratio of 2:1, and the mixture was then immediately loaded on the lower plate (DMEM was added to trigger the self-assembly of the peptides in solution to form a hydrogel). During this process, the storage (elastic) modulus ($G'$) and loss (viscous) modulus ($G''$) of the designer self-assmebling peptides were evaluated in the frequency sweeps ranging from 0.1 rad/s to 100 rad/s, which were performed at a constant shear stress of 1 Pa at 37 °C.

**2.5. Preparation of Human Degenerated Nucleus Pulposus Cells (hdNPCs).** The approval of the ethics committee and the informed consent of the patient were obtained. Degenerated human NP tissue was obtained from disc level L4-L5 of a 48-year-old man who had undergone a fusion surgery due to lumbar-disc herniation (Pfirrmann grade V). After washing the specimen twice using phosphate-buffered saline (PBS, Gibco), the annulus fibrosus and cartilaginous end plates were carefully removed, and the hdNPCs were isolated as previously described. Briefly, the NP tissue was cut into approximately 1 $mm^3$ pieces, which were then digested using a solution of 0.025% of collagenase type II (Sigma) in serum-free medium at 37 °C in 5% $CO_2$. After 8 h, the cells were pelleted by centrifugation at 400$g$ for 6 min. The supernatant was removed and the cells were resuspended and cultured in a 25 $cm^2$ flask in DMEM/F12 containing 10% fetal bovine serum (FBS, Gibco), 100 U/mL penicillin, 100 mg/mL streptomycin, and 2.5 mg/mL amphotericin B. The culture medium was changed every 2−3 days.

**2.6. Three-Dimensional Cell Culture in Self-Assembling Peptide Scaffolds.** Transwell inserts were first placed into a 24-well culture plate, and 400 $\mu$L of culture medium was added to each well. The hdNPCs were suspended in 10% sucrose before seeding. A 20 $\mu$L aliquot of cell suspension containing 1 × $10^5$ hNPCs was quickly mixed with 100 $\mu$L of the peptide solution, and then the cell/peptide mixture was immediately placed in the inset. A 400 $\mu$L aliquot of culture medium was very slowly added to the surface of each hydrogel, gelation at was allowed to proceed at 37 °C for 10 min, and then the medium was changed for another 30 min of incubation. The medium was changed at least twice to enhance peptide self-assembly and to equilibrate the pH. Subsequently, the medium was changed every 2 days.

**2.7. Scanning Electron Microscopy (SEM) Assessment.** All of the self-assembling peptide hydrogel scaffolds and cell/scaffolds were cultured for 7 days and 14 days. Then, the microstructures of and the cellular attachments to these scaffolds were observed using SEM. All of the samples were fixed, dehydrated, and coated with platinum. The images were captured using a JEOL SEM at 800−24 000 × magnification at a voltage of 20 kV.

**2.8. Three-Dimensional Cell-Migration Assessment.** All of the self-assembling peptide hydrogel scaffolds were prepared as above-described, and 2 × $10^4$ hdNPCs in 400 $\mu$L of culture medium were seeded on the top of the scaffolds. These preparations were transferred to a new 12-well culture plate with 800 $\mu$L of culture medium in each well. After 1, 4, and 7 days, the hdNPCs in the peptide hydrogels were labeled using the fluorogenic ester calcein-AM (CAM, Dojinda, Japan). Briefly, the cells/scaffolds were incubated with 2 $\mu$mol/L CAM for 30 min at room temperature in the dark and then gently rinsed three times using PBS. Images were collected using a laser confocal microscope (LCM, FV500, Olympus, Japan) through scanning a Z-stack with a step size of 3 $\mu$m, and 3D reconstructions were prepared using NIH ImageJ to show the cells that had migrated into the peptide hydrogels. These experiments were repeated three times.

**2.9. Cell Cytotoxicity Assessment.** An aliquot of 1 × $10^5$ hdNPCs were 3D cultured in each of the self-assembling peptide hydrogel scaffolds. After 1, 4, and 7 days, the live and dead hdNPCs were labeled using CAM and the nucleic acid dye propidium iodide (PI, Sigma, U.S.A.), respectively. Briefly, the cells/scaffolds were incubated with 2 $\mu$mol/L CAM and 5 $\mu$mol/L PI for 30 min at room temperature in the dark, and then they were gently rinsed three times using PBS. The images were collected using laser confocal microscopy, and the number of live cells and dead cells in five randomly selected nonoverlapping areas were counted by two independent assessors. The experiments were performed in triplicate.

**2.10. Cell Proliferation Assessment.** A sample of 2 × $10^4$ hdNPCs was 3D cultured in individual peptide hydrogels in 48-well culture plates containing medium with or without 10 ng/mL BMP7 as the negative control group (NCG) and positive control group (PCG), respectively. After 1, 3, 5, and 7 days, the number of cells was evaluated using cell counting kit-8 reagents (CCK-8, Dojindo, Japan). The absorbance at 450 nm, which indirectly reflected the number of cells, was measured using a microplate reader (Elx800, Bio-Tek, U.S.A.). The experiments were repeated three times.

**2.11. Enzyme-Linked Immunosorbent Assay (ELISA) of ECM Secretion.** A sample of 1 × $10^5$ hdNPCs was 3D cultured in individual peptide hydrogels in 48-well culture plates containing culture medium with or without 10 ng/mL BMP7, as the NCG and the PCG, respectively. After 7, 14, and 28 days, the total amounts of aggrecan and collagen II that had been secreted by the hdNPCs were determined using ELISA kits according to the manufacturer's protocols (R&D System, MN, U.S.A.). The ELISA data were normalized to the cell numbers determined using CCK-8 to evaluate the ECM-secreting ability of the cells. The experiments were repeated three times.

**2.12. Quantitative Real-Time PCR (qRT-PCR) Analysis of Gene Expression.** A sample of 1 × $10^5$ hdNPCs was 3D cultured in individual peptide hydrogels in 48-well culture plates containing culture medium with or without 10 ng/mL BMP7, as the NCG and the PCG, respectively. After 7, 14, and 28 days, the cells were disrupted mechanically, and the total RNA was extracted using TRIzol (Invitrogen, U.S.A.) reagent according to the manufacturer's instruction. Then, cDNA was obtained from the total RNA using a reverse transcription reagent (SYBR Premix Ex Taq, Takara, Japan).


DOI: 10.1021/acsami.5b03605
ACS Appl. Mater. Interfaces 2015, 7, 17076−17087

**Table 2. Nucleotide Sequences of the Primers for Quantitative Real-Time Polymerase Chain Reaction**

| gene | gene bank | forward sequence | reverse sequence |
|---|---|---|---|
| GAPDH | NM_000576.2 | GAAGGTCGGAGTCAACGG | GGAAGATGGTGATGGGATT |
| collagen type I $\alpha$1 | NM_000088.3 | CCTGGAAAGAATGGAGATGATG | ATCCAAACCACTGAAACCTCTG |
| collagen type II $\alpha$1 | NM_001844.4 | GGTAAGTGGGGCAAGACTGTTA | TGTTGTTTCTGGGTTCAGGTTT |
| collagen type X $\alpha$1 | NM_000493.3 | GTGTTTTACGCTGAACGATACC | TGGTGTAGGGAATGAAGAACTG |
| Sox-9 | NM_000346.3 | GCCTCTACTCCACCTTCACCTA | GCTGTGTGTAGACAAGTTGTT |
| aggrecan | NM_001135.3 | GTCAGATACCCCATCCACACTC | CATAAAAGACCTCACCCTCCAT |
| versican | NM_001126336.2 | GTAACCCATGCGCTACATAAAGT | GGCAAAGTAGGCATCGTTGAAA |

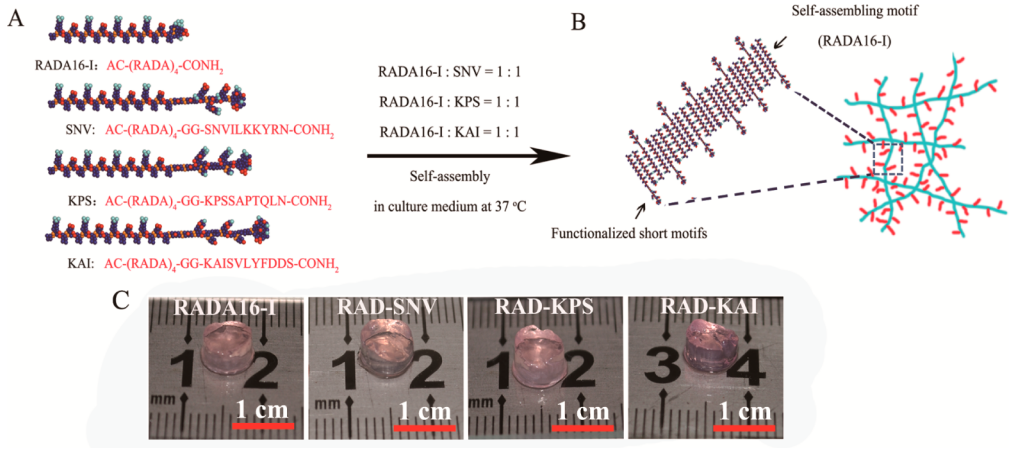


**Figure 1.** (A) Molecular models of the designer self-assembling peptides and functionalized self-assembling peptides. (B) Schematic illustrations of nanofiber formation by the self-assembling peptides after being mixed with RADA16-I. (C) The designer self-assembling peptides self-assembled to form nanofibrous hydrogel scaffolds under physiological conditions via alternating hydrophobic and hydrophilic amino acids in vitro.

After the cDNA had been acquired, the expression levels of the NPC-related genes (those encoding collagen I $\alpha$1, collagen II$\alpha$1, collagen X, aggrecan, sox-9, and versican) were analyzed using qRT-PCR, using the glyceraldehyde-3-phosphate dehydrogenase (GAPDH) housekeeping gene as the control. The primers for all of the genes were designed using Premier 5.0 software and are shown in Table 2. A SYBR Premix Ex Taq PCR kit (Takara, Japan) and Mini OpticonTM Detector system (Bio-Med, U.S.A.) were used for the qRT-PCR analysis. After a cycle of 95 °C for 20 s, the samples were cycled 40 times at 95 °C for 5 s and 60 °C for 20 s. Then, a cycle threshold (Ct) value was obtained for each sample, and the values of triplicate samples were averaged. The $2^{-\Delta\Delta Ct}$ values were used to evaluate the relative expression levels of the genes. All of the data were acquired in three independent experiments in which each sample was evaluated in triplicate.

**2.13. In Vivo Compatibility Test.** KM mice (25−20 g) were used for the in vivo test. The in vivo biocompatibility study was performed in accordance with the guidelines of the Council on Animal Care of the Navy General Hospital. The KM mice were anesthetized, and their fur and skin were sterilized, and then 100 $\mu$L of RAD-KPS was subcutaneously injected into their dorsal region. Four mice were sacrificed at 3, 14, and 28 days after injection. Then, the tissue reactions were evaluated using H&E staining.

**2.14. Statistical Analysis.** All the data were statistically analyzed using SPSS 13.0 software and are presented as the mean values ± standard deviation. An ANOVA of factorial design was performed to analyze the main effect and the interaction between the groups and the time periods, a one-way ANOVA was performed for multiple-group comparisons, and the Student−Newman−Keuls' test (homogeneity of variance) or the Tamhane's test (heterogeneity of variance) was performed to compare any two groups. A $P$ value of <0.05 was considered to indicate a significant difference.

## 3. RESULTS

**3.1. Synthesis of Designer Peptides and Hydrogel Formation.** The designer peptides were synthesized by extending the C-terminus of the self-assembling peptide RADA16-I to include each of the functional motifs of BMP7. Two glycine residues were used as a spacer linker to maintain the flexibility of the functionalized self-assembling peptides. A schematic illustration of the functional peptides is shown in Figure 1A,B. After being incubated in culture medium in 37 °C, all of the peptides (RADA16-I, RAD-SNV, RAD-KPS, and RAD-KAI) self-assembled to form transparent viscous hydrogel-like scaffolds (Figure 1C) and were therefore suitable for microscopic analyses.

**3.2. Microstructural Study of Designer Peptides.** To determine the secondary structure of the self-assembling peptides that formed hydrogels, 25 mM solutions were examined using CD spectroscopy. As shown in Figure 2, a typical spectrum of $\beta$-sheet structures was obtained for RADA16-I, with a positive maximum molar residue ellipticity (deg cm$^2$/decimole) at 195 nm and a negative maximum molar residue ellipticity at 216 nm. Furthermore, these typical $\beta$-sheet structures were also observed in the functionalized self-assembling peptide mixture solutions. However, compared with those of the pure RADA16-I solutions, the intensities of the molar residue ellipticity at 216 and 195 nm of the functionalized peptide mixture solutions were decreased, and the $\beta$-sheet contents were reduced.

We first observed nanofiber formation by RADA16-I, RAD-SNV, RAD-KPS, and RAD-KAI using AFM. As shown in Figure


DOI: 10.1021/acsami.5b03605
ACS Appl. Mater. Interfaces 2015, 7, 17076−17087

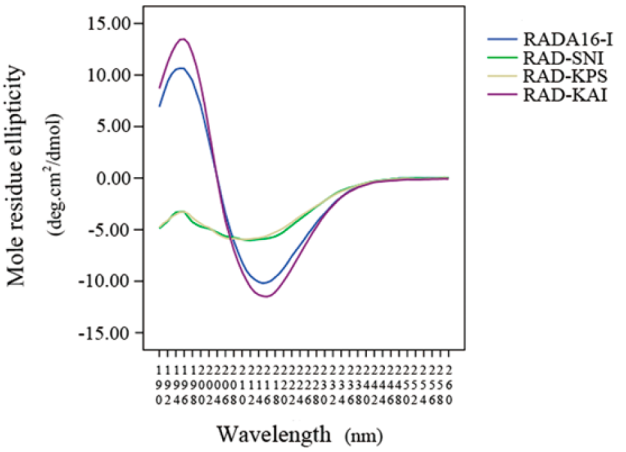


**Figure 2.** CD spectra of the designer self-assembling peptide solutions. All of the peptides in solution formed typical $\beta$-sheet structures.

3, both RADA16-I and the functionalized self-assembling peptides formed numerous nanofibers, with lengths ranging

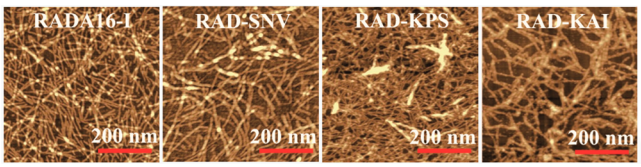


**Figure 3.** Atomic force microscopy (AFM) images of the designer self-assembling peptides. The AFM results showed that nanofiber formation occurred in of all of the solutions of the self-assembling peptides.

from several hundreds of nanometers to a few micrometers. However, the diameters of the nanofibers assembled from the functionalized peptide mixtures were thicker than those of pure RADA16-I ($p < 0.05$). The average diameters of the nanofibers in the RADA16-I, RAD-SNV, RAD-KPS, and RAD-KAI solutions were 15.2 ± 2.1, 48.7 ± 11.7, 26.1 ± 9.3, and 51.8 ± 10.8 nm, respectively.

**3.3. Rheological Study of the Designer Peptides.** The frequency sweep results (Figure 4) obtained at 37 °C revealed that the viscoelasticity of all four of the hydrogels was similar (including the storage modulus and loss modulus values), and

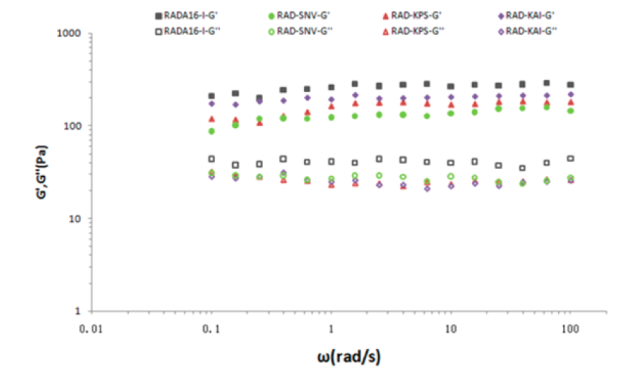


**Figure 4.** Results of the oscillation frequency sweep data on 1% (w/v) of the designer self-assembling peptides with DMEM at 37 °C. A typical gel-like behavior was evident as the storage modulus ($G'$, 100 Pa) values of the four hydrogels were higher than the loss modulus ($G''$, 10 Pa) values in the range of the shear rate frequencies, and both $G'$ and $G''$ were independent of the shear rate frequency.

both $G'$ and $G''$ were independent of the shear rate frequency. A typical gel-like behavior was evident as the storage modulus ($G'$, 100 Pa) values of the four hydrogels were approximately 1 order of magnitude greater than the loss modulus ($G''$, 10 Pa) values in the range of the shear rate frequencies. In addition, the values of $G'$ and $G''$ in RADA16 were greater than the other three functionalized self-assembling peptides in the range of shear rate frequencies, whereas the values of $G'$ and $G''$ of the three functionalized self-assembling peptides were similar.

**3.4. Cell Attachment to the Designer Peptide Hydrogel Scaffolds.** After gelation, SEM was first used to observe the microstructures of the self-assembling peptide hydrogel scaffolds. The SEM images (Figure 5A,B) confirmed that all of the peptides

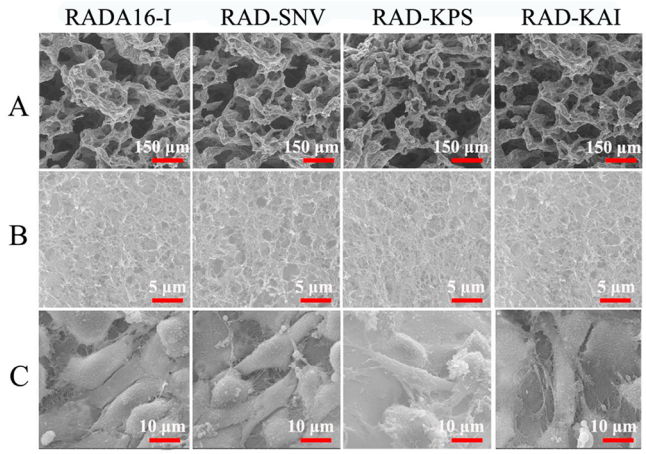


**Figure 5.** Scanning-electron microscopy (SEM) images of the designer self-assembling peptides. The SEM images showed that all of the designer self-assembling peptides had formed nanofibers that had interwoven to form porous structures (A: before hydration; B: after hydration) and that the hNPCs had attached to the nanofibers by extending many pseudopodia (C, white arrows).

could self-assemble to form nanofibers and further interweaved to form porous structures, which were very similar to that of the natural ECM, with fibers of ~40 nm in diameter and pores ranging from 5 to 200 nm in diameter. In addition, to examine the cell−scaffold interactions, hdNPCs were 3D cultured in these designer peptide hydrogel scaffolds, and SEM analysis was performed. As shown in Figure 5C, the hdNPCs had fully embedded in all of the self-assembling peptide hydrogel scaffolds and had tightly attached to the nanofibers via extending many pseudopodia. Moreover, abundant ECM-like substances were observed on the surface of the hdNPCs after they had been 3D cultured for 14 days.

**3.5. Cell Migration into the Designer Peptide Hydrogel Scaffolds.** The typical morphology of hdNPCs cultured on the surface of the designer peptide hydrogel scaffolds are shown in Figure 6A. The cells exhibited a similar morphology in all of the peptide scaffolds, with strong adhesion to the nanofibers, and gave rise to cell clusters. A greater number of cell clusters were observed in the RAD-SNV and RAD-KPS scaffolds than in RADA16-I and RAD-KAI scaffolds. Furthermore, the spontaneous migration of the hdNPCs in response to the various peptide hydrogel scaffolds were studied through reconstructing 3D microscopic images (Figure 6B). All of the peptide hydrogel scaffolds promoted 3D migration of the hdNPCs for several hundred micrometers. However, the distances that the cells in the RAD-SNV (290.6 $\mu$m) and RAD-KPS (295.8 $\mu$m) scaffolds


DOI: 10.1021/acsami.5b03605
ACS Appl. Mater. Interfaces 2015, 7, 17076−17087

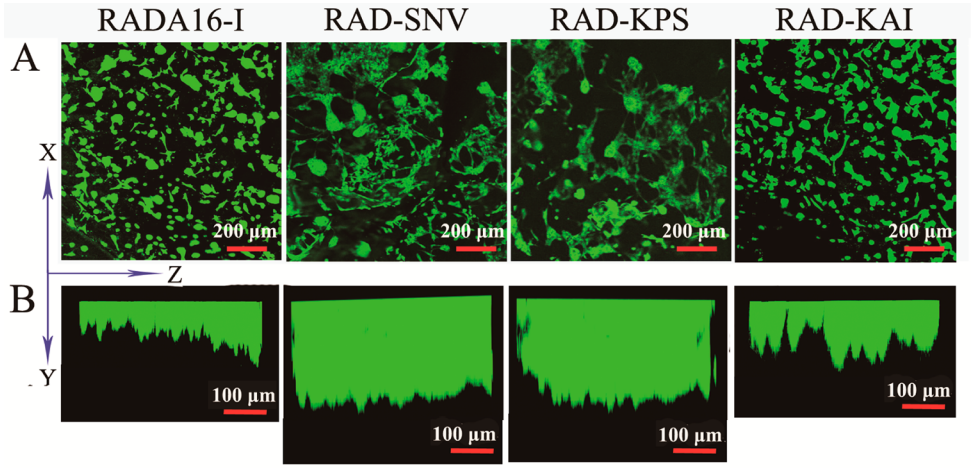


**Figure 6.** Human degenerated NPCs 3D cultured on the surface of the designer self-assembling peptide hydrogel scaffolds (A) and migrated into the hydrogel scaffolds (B) after 7 days.

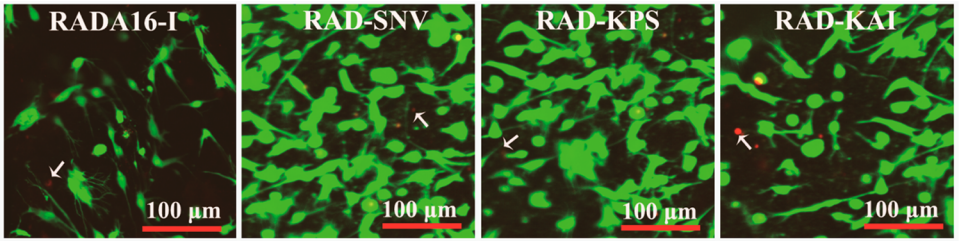


**Figure 7.** Live/dead cell viability assay for hNPCs that were 3D cultured in the designer self-assembling peptide hydrogel scaffolds for 7 days. The green fluorescent cells are the live cells labeled with CAM, and the red fluorescent cells are the dead cells labeled with PI.

migrated were significantly longer than those of the cells in the RADA16-I (118.3 $\mu$m) and RAD-KAI (182.7 $\mu$m) scaffolds.

**3.6. Cell Viability in the Designer Peptide Hydrogel Scaffolds.** The viability of hdNPCs 3D cultured in the self-assembling peptide nanofibrous hydrogel scaffolds was determined using the Live/Dead cell viability assay. As shown in Figure 7, the survival rate of hdNPCs that were 3D cultured in each of the self-assembling peptide hydrogel scaffolds was greater than 90% after 7 days. These results suggested that RADA16-I had extremely weak toxicity for the hdNPCs and that the functional short motifs did not increase the cytotoxicity level (Figure 8, $p > 0.05$).

**3.7. Cell Proliferation in the Designer Peptide Hydrogel Scaffolds.** The CCK-8 assay was used to quantitatively analyze the population of hdNPCs that were 3D cultured in each of the peptide hydrogel scaffolds. Figure 9 shows that the number of cells in each of the scaffolds and the control groups increased over time. However, the proliferation rates of the cell in the self-assembling peptide hydrogel scaffolds were significantly higher than those of the 2D-cultured control groups ($p < 0.01$), and there was no obvious difference between the NCG and PCG rates ($p > 0.05$). Furthermore, the proliferation rate of hdNPCs cultured in RAD/SNV and RAD-KPS scaffolds were obviously higher than those in RADA16-I and RAD-KAI scaffolds. After being cultured for 7 days, the number of cells in the positive control group and the RADA16-I, RAD-SNV, RAD-KPS, and RAD-KAI group were 1.13, 1.88, 2.47, 2.58, and 1.74 times as many as those in the negative control group, respectively. Moreover, there was no significant difference between the number of cells in the RADA16-I and RAD-KAI groups or

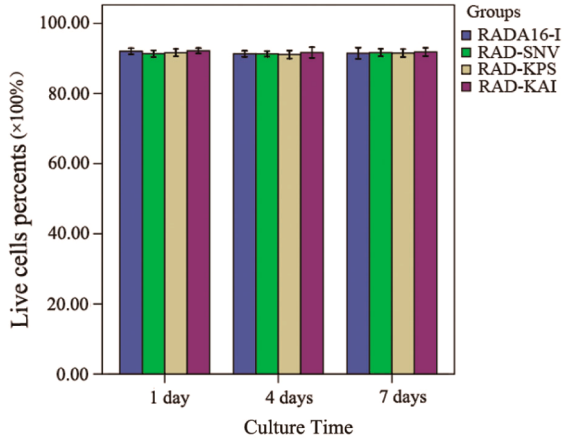


**Figure 8.** Quantification of the survival rates of hNPCs that were 3D cultured in the designer self-assembling hydrogel scaffolds for 7 days. The survival rates of hdNPCs did not have statistical difference among the designer self-assembling hydrogel scaffolds.

between those in the RAD-SNV and RAD-KAI groups ($p > 0.05$).

**3.8. ECM Secretion in the Designer Peptide Hydrogel Scaffolds.** ELISA assays were used to quantitatively determine the amount of ECM (aggrecan and collagen II) secreted by hdNPCs that were 3D cultured in the designer peptide hydrogel scaffolds. The total amounts of collagen II and aggrecan secreted were then normalized to the number of cells present to evaluate the secretory ability per hdNPC. As shown in Figure 10, the designer peptide hydrogel scaffolds dramatically improved the collagen II- and aggrecan-secretory abilities of hdNPCs


DOI: 10.1021/acsami.5b03605
ACS Appl. Mater. Interfaces 2015, 7, 17076−17087

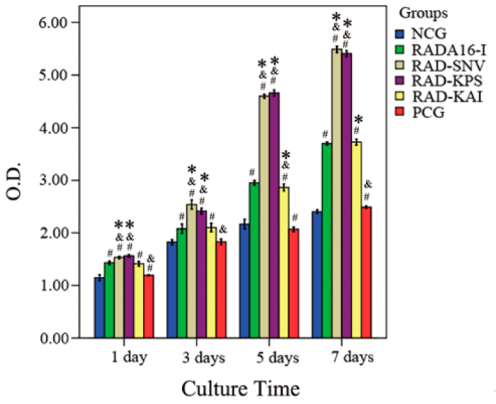


**Figure 9.** CCK-8-based quantification of the proliferation rates of hNPCs that were 3D cultured in the designer self-assembling peptide scaffolds for 1, 3, 5, and 7 days. NCG: hNPCs cultured in cell culture plates without BMP7. PCG: hNPCs cultured in cell culture plates with BMP7. The following symbols indicate significant differences: $p < 0.05$: # compared to the NCG; & compared to the RADA16-I group; and * compared to the PCG.

compared with those of the NCG ($p < 0.01$) during the culture period, but these abilities were significantly lower than those of the PCG ($p < 0.01$). The differences appeared mainly during the first 14 days, particularly during the first 7 days, and were maintained for at least 28 days. After being cultured for 28 days, both the collagen II and aggrecan-secretory abilities of the hdNPCs grown in the RAD-SNV and RAD-KPS scaffolds were significantly higher than those of cells grown in the RADA16-I and RAD-KAI scaffolds ($p < 0.01$), whereas there was no obvious difference in the collagen II- and aggrecan-secretory abilities of hdNPCs grown in the RADA16-I or RAD-KAI scaffolds ($p > 0.05$). Moreover, there was no obvious difference in the collagen II-secretory abilities of hdNPCs grown in RAD-SNV or RAD-KPS scaffolds for 14 days ($p > 0.05$), whereas the aggrecan-secretory ability of hdNPCs grown in the RAD-KPS scaffold was significantly higher than that of cells grown in the RAD-SNV scaffold for this period ($p < 0.05$).

**3.9. Gene Expression in the Designer Peptide Hydrogel Scaffolds.** To evaluate the effect of the functionalized peptide hydrogel scaffolds on the expression of relevant genes (genes encoding collagen I $\alpha$1, collagen II $\alpha$1, collagen X, sox-9, aggrecan, and versican), the expression levels were analyzed after 7, 14, and 28 days of culture using qRT-PCR, using GAPDH expression as the control. The results were expressed as the levels of gene expression relative to those of the NCG. As shown in Figure 11, compared to the NCG levels, the levels of collagen

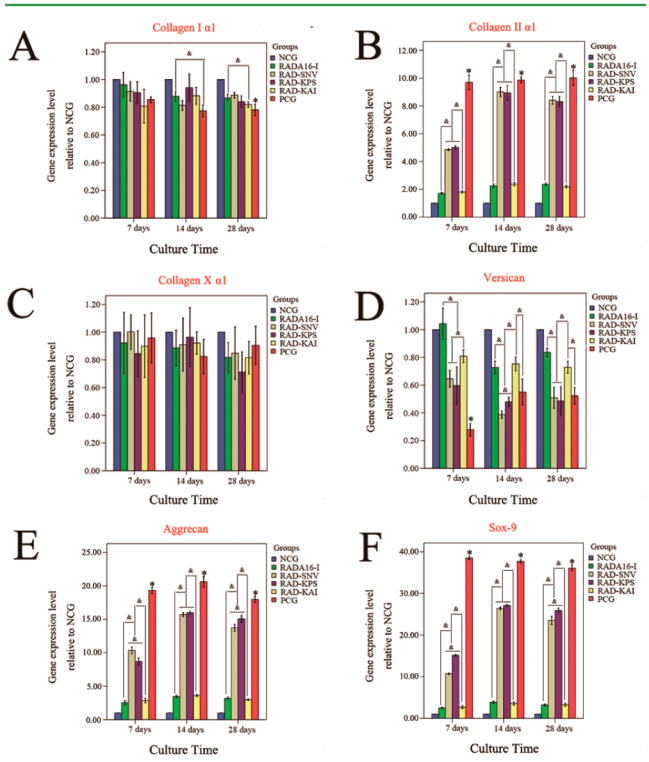


**Figure 11.** Quantification of the levels of gene expression by hNPCs that were 3D cultured in the designer self-assembling peptide scaffolds for 7, 14, and 28 days, as determined using qRT-PCR. NCG: hNPCs cultured in cell culture plates without BMP7. PCG: hNPCs cultured in cell culture plates with BMP7. & indicates $p < 0.05$; # indicates $p < 0.05$ when the NCG was compared with the other groups; * indicates $p < 0.05$ when the PCG was compared with the other groups.

II$\alpha$1, sox-9, and aggrecan mRNA expression were significantly increased, those of collagen I$\alpha$1 and versican mRNAs were obviously decreased in all the designer peptide hydrogel scaffold groups ($p < 0.05$), and there were no significant differences in the levels of collagen X$\alpha$1 mRNA expression among the groups ($p > 0.05$). Moreover, these changes in RAD-SNV and RAD-KPS groups were more significant than those in RADA16-I and RAD-KAI groups ($p < 0.05$) but less than those in PCG ($p < 0.05$). The

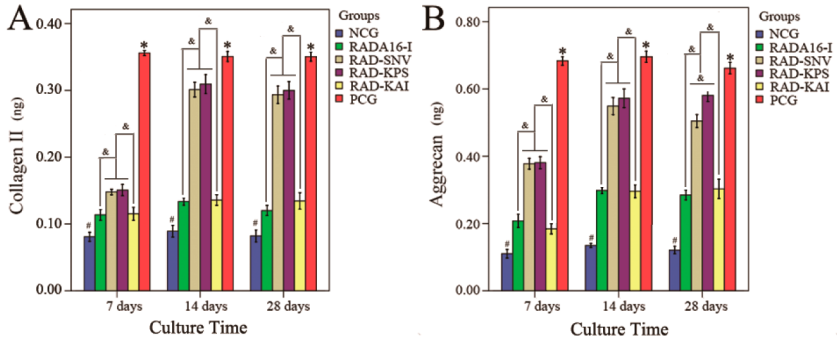


**Figure 10.** Collagen II- and aggrecan-secretory abilities of hNPCs 3D cultured in the designer self-assembling peptide scaffolds for 7, 14, and 28 days, as determined using ELISA assays. NCG: hNPCs cultured in cell culture plates without BMP7. PCG: hNPCs cultured in cell culture plates with BMP7. & indicates $p < 0.05$; # indicates $p < 0.05$ when the NCG was compared with the other groups; * indicates $p < 0.05$ when the PCG was compared with the other groups.


DOI: 10.1021/acsami.5b03605
ACS Appl. Mater. Interfaces 2015, 7, 17076−17087

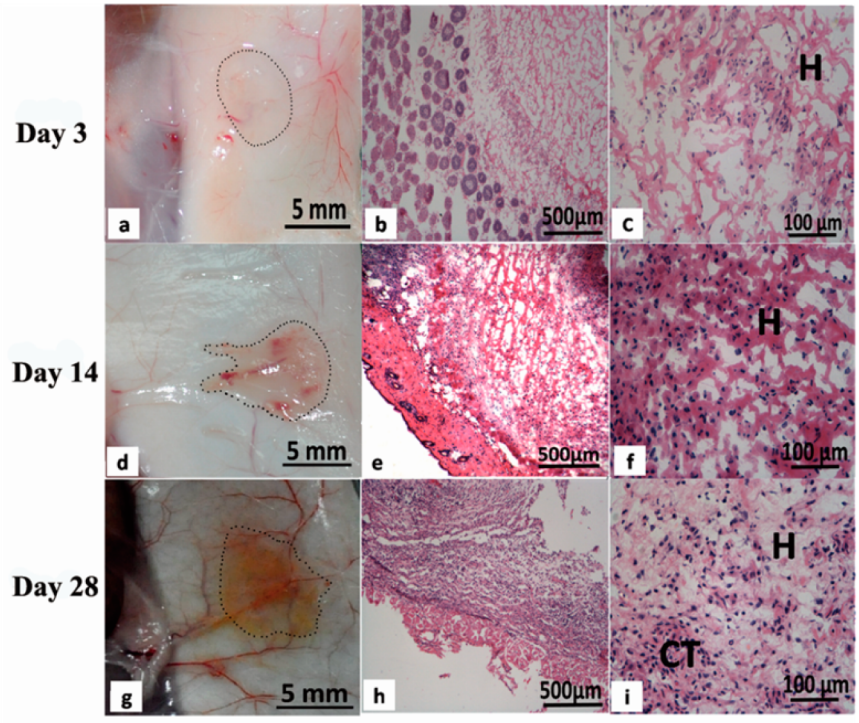


**Figure 12.** Macroscopic (a, d, and g) and microscopic views (H&E-stained sections, b, c, e, f, h, and (i) of the tissue response on days 3, 14, and 28 after RAD-KPS was subcutaneously injected. (H: hydrogel, CT: connective tissue).

results also showed that these differences also occurred mainly within the first 14 days and were maintained for at least 28 days.

After being cultured for 28 days, there were no significant differences in any of the levels of mRNA expression of the RADA16-I and RAD-KPS groups except for that of collagen I$\alpha$1 ($p > 0.05$). Moreover, there also were no obvious differences in the levels of expression of collagen I$\alpha$1, collagen II$\alpha$1, collagen X$\alpha$1, and versican mRNAs by hdNPCs grown in the RAD-SNV or the RAD-KPS scaffolds ($p > 0.05$). However, the levels of aggrecan and sox-9 mRNA expression by hdNPCs grown in the RAD-KPS scaffold were significantly higher than those of cells grown in the RAD-SNV scaffold ($p < 0.05$).

**3.10. In Vivo Degradation and Biocompatibility.** The in vivo gelatinization and degradation of the RAD-KPS material were observed in KM mice. On day 3 after injection, RAD-KPS had formed a round-shaped transparent protrusion with a vague boundary with the surrounding tissue (Figure 12a). The overall size of the protrusion had decreased by approximately half by day 14 (Figure 12d) by one-third by day 28(Figure 12g).

In studying the images of H&E-stained tissues, minor inflammatory infiltration on the edge of the hydrogel scaffold was observed (Figure 12b,c) on day 3. At 14 days after injection, large numbers of inflammatory cells, such as eosinophils, neutrophils, and macrophages, were found to have infiltrated the center of the hydrogel scaffold and degradation of the marginal area of the scaffold was observed (Figure 12e,f). At 28 days after injection, the inflammatory reaction was attenuated, with a reduced number of macrophages and a significant increase in the number of fibroblasts observed. In addition, the RAD-KPS scaffold had partially degraded and was being gradually replaced by connective tissue (Figures 12h,i).

## 4. DISCUSSION

The ideal aim in repairing IDD is to induce regeneration of the degenerated NP in situ. A tissue engineering strategy is considered one of the most promising approaches to the treatment of IDD.[36] The biomaterial that is a delivery vehicle for the cells is very important in NP tissue engineering. An ideal biomaterial scaffold for human degenerated NP tissue engineering should have at least the following three characteristics: good biocompatibility, excellent bioactivities, and injectability.[37] The self-assembling peptide RADA16-I is a promising scaffold material that exhibited a strong potential for applications in various fields of tissue engineering.[27,28,38] Therefore, in the present study, we conjugated three different short functional motifs of BMP7 to the C-terminus of the RADA16-I using solid-phase synthesis to obtain novel functionalized self-assembling peptides that would support hdNPC growth. Analysis of the migration, proliferation, and ECM secretion of hdNPCs grown on the BMP7-functionalized self-assembling peptide nanofibrous hydrogels showed that they were satisfactory 3D scaffolds for hdNPC growth.

Although the self-assembling peptide RADA16-I has been widely used in various types of tissue engineering, it lacks tissue specificity. Many studies have demonstrated that the tissue-specific biological function of peptide scaffolds could be significantly improved by conjugating a specific short functional peptide to the main peptide of RADA16-I.[23,28,39] In this study, we conjugated the functional short motifs of BMP7 to the C-terminus of RADA16-I to obtain NP tissue-specific functionalized self-assembling peptides. Chen et al.[34] have demonstrated that these short motifs (SNV, KPS, and KAI) were the important short functional peptides of BMP7 and that they could be easily used to chemically functionalize nanofibrous biomaterials. Furthermore, combinations of these short peptides were more suitable for osteoblasts than were the individual peptides.


DOI: 10.1021/acsami.5b03605
ACS Appl. Mater. Interfaces 2015, 7, 17076−17087

However, Gelain et al.[29] noted that self-assembly and nanofiber formation might be inhibited if the functional motifs extended the self-assembling peptide RADA16-I by more than 12 additional residues. Therefore, we separately conjugated only the three short functional motifs (≤11 amino acids) of BMP7 to the C-terminus of RADA16-I.

Our previous study demonstrated that KPS could be conjugated to the C-terminus of RADA16-I (RKP) but that this affected the $\beta$-sheet structures, which are very important and necessary for peptide self-assembly and nanofiber formation.[35] Only when KPS was mixed with RADA16-I at an equal volume ratio (RAD-KPS) were the $\beta$-sheet structures regained. Furthermore, our previous study also showed that RAD-KPS was more suitable for NP tissue engineering applications than was pure RKP. Therefore, in this study, we first conjugated SNV, KPS, and KAI to the C-terminus of RADA16-I, and then mixed each of these with RADA16-I at a volume ratio of 1:1 to form three novel functionalized self-assembling peptides, RAD-SNV, RAD-KPS, and RAD-KAI. The results showed that all of these functionalized peptides could self-assemble to form hydrogel-like scaffolds through their $\beta$-sheet secondary structures, even though the peak values were less than those of pure RADA16-I (Figure 2).

It is critical that the biomaterial scaffold for NP tissue-regeneration applications closely mimics the NP-like 3D microenvironment. In our study, the results of both the AFM (Figure 3) and SEM analyses (Figure 5) demonstrated that all of the designer peptides could form numerous long nanofibers and higher-order interwoven 3D nanofibrous networks with fibers of ~40 nm in diameter, pores ranging from 5 to 200 nm and an extremely high water content (>99 wt % water). These nanofibrous structures were significantly smaller than the hdNPCs and could provide a natural ECM-like 3D microenvironment for them. Moreover, nanofibrous networks are beneficial for the diffusion of nutrients and excretion of metabolites. This aspect is particularly important for NP tissue engineering applications due to the lack of nutrients in NP tissue. We also observed that hdNPCs could adhere to the nanofibers of all of the designer peptide hydrogel scaffolds through extending many pseudopodia (Figure 5C) and that all of the designer peptide hydrogel scaffolds had extremely low cytotoxicity for the hdNPCs (Figure 7). These results suggested that all of the designer peptide nanofibrous hydrogel scaffolds possess excellent biocompatibility with hdNPCs in vitro and had the potential for NP tissue engineering applications.

Compared with that of the pure RADA16-I group, the results showed that the RAD-SNV and RAD-KPS functionalized peptide hydrogel scaffolds significantly increased the migration (Figure 6B) and proliferation (Figure 9) of hdNPCs, their secretion of collagen II and aggrecan (Figure 10), and upregulated their expression of collagen II $\alpha$, aggrecan, and sox-9 mRNAs (Figure 11). There were no obvious differences between the values for the RADA16-I and RAD-KAI groups, and the levels of aggrecan secretion and the expression of aggrecan and sox-9 mRNAs were obviously highest in the RAD-KPS scaffolds among the three functionalized peptide hydrogel scaffolds. These findings indicated that the functional short motifs SNV and KPS of BMP7 obviously improved the bioactivities of RADA16-I toward hdNPCs in vitro and that KPS may have the strongest effects on the hdNPCs. However, these results differ from the results obtained using short peptides for osteoblast growth. Studies using osteoblasts showed that the short peptide KPS promoted their highest cell proliferation rate and that KAI most strongly enhanced their calcium deposition.[34] These results suggested that the functional short motifs of BMP7 have different effects on different cells. All of the short motifs of BMP7 that were used to design the functionalized self-assembling peptides improved the bioactivities of hdNPCs, with RAD-SNV and RAD-KPS being more suitable for NP tissue-engineering applications and RAD-KPS appearing to have more potential than did RAD-SNV.

To further evaluate the ability of the functionalized self-assembling peptide hydrogel scaffolds to promote the bioactivities of hdNPCs, we used hdNPCs cultured in medium containing BMP7 as the positive control group. The results showed that the proliferation rate of hdNPCs was obviously lower in the PCG than in any of the designer self-assembling hydrogel scaffold groups (Figure 9), whereas the level of ECM secretion was significantly higher in the PCG than in any of the designer self-assembling hydrogel scaffold groups (Figure 10, 11). These results indicated that the BMP7 promoted the bioactivities of hdNPCs mainly through enhancing the secretion of ECM components by individual hdNPCs but not through increasing the proliferation rate of hdNPCs, which is consistent with the results of other studies.[12,40] However, the functionalized self-assembling peptide hydrogels not only improved the total amount of ECM components secreted by increasing the proliferation rate of hdNPCs (Figure 9) but also enhanced the ECM-secretory ability of individual hdNPCs (Figure 10). We speculated that the higher proliferation rate of hdNPCs grown in the designer self-assembling peptide hydrogels was primarily due to the scaffolds providing a 3D environment for easy passage, whereas the enhanced ECM-secretory ability of individual hdNPCs in the RAD-SNV and RAD-KPS scaffolds was mainly caused by the presence of the short BMP7 motifs SNV and KPSS. Although the levels of ECM-component secretion were significantly higher in the PCG than were those of the functionalized self-assembling peptide hydrogel scaffold groups, BMP7 had to be added to the culture medium every 2 days during the 28-day period due to its disadvantageously short half-life. Moreover, for its clinical application, BMP7 would have to be injected into the degenerated disc many times to maintain the levels of its bioactivities, which is not realistic. However, in this study, we found that the bioactivities of BMP7 could be improved via prolonged release by utilizing its short functional motifs as C-terminal conjugates of RADA16-I and that these functionalized peptides self-assembled to form nanofibrous hydrogel scaffolds via $\beta$-sheets under physiological conditions (Figure 2). Because the chemical bonds formed under this condition were obviously stronger than those formed when using the traditional physical soaking methods, the functional motifs, particularly SNV and KPS, could be slowly released to increase the rate of ECM secretion for at least 28 days. Therefore, the functionalized self-assembling peptides RAD-SNV and RAD-KPS have a better potential for clinical applications than does BMP7. These peptides could be injected into a disc one time and maintain their bioactivities for a long period.

As described above, RAD-SNV and RAD-KPS exhibited more bioactivities for hdNPCs than did RAD-KAI, and the levels of aggrecan secretion and the expression of aggrecan and sox-9 mRNAs were significantly higher in RAD-KPS scaffolds than those observed in RAD-SNV scaffolds in vitro. Thus, we chose the better one, RAD-KPS, for the in vivo compatibility evaluation. Following subcutaneous injection, the RAD-KPS material gelled within 1 min, forming a structure of approximately 5 mm in diameter and 3 mm thick (data not


DOI: 10.1021/acsami.5b03605
ACS Appl. Mater. Interfaces 2015, 7, 17076−17087

shown). The integrity of the RAD-KPS structure was maintained for up to 14 days, but its size decreased gradually. The eosinophil, neutrophil, and macrophage infiltrates observed in H&E-stained sections showed that an acute inflammatory reaction was occurring on days 3 and 14. However, the number of infiltrated inflammatory cell had decreased significantly by day 28, and the acute inflammation gradually became a chronic inflammation characterized by fibroblast infiltration and connective tissue formation. The degradation rate and the rate of its replacement by newly formed tissue were similar to those of other biocompatible hydrogel scaffolds.[41,42] Therefore, these results indicated that the RAD-KPS was biocompatible in vivo and is thus suitable for use in intervertebral disc repair.

The IVD is a complex tissue that includes the NP, the annulus fibrosus (AF), and the cartilage end plate (CE), and the main function of an IVD is to support spinal movement and act as an absorber. However, the distinct regions of the IVD have developed to performed different roles when the spine bears complex loads.[43] The central NP is a gel-like substance. Compressive loads are borne primarily by the NP, which must be aided by the surrounding AF. Torsional and bending loads are borne mainly by the AF.[44] Furthermore, the functional roles of the NP in elasticity and deformation under stress are directly due to its high content of proteoglycans, which foster its hyper-hydrated state.[45] Thus, an intact AF and the proteoglycan content of the NP are critical for the NP to bear mechanical loading. If the AF was mostly intact, cells injected into a degenerated NP, even without biomaterials, could ameliorate intervertebral disc degeneration by increasing the ECM and water contents. However, if the AF was damaged, even the natural NP, presumed to be the ideal implant material, was not able to restore the mechanical functionality of the IVD.[46]

In this study, we found that the BMP7-based functionalized peptides could self-assemble to form NP-like nanofibrous hydrogels (as shown in Figure 1C). From the rheological results of the designed self-assembling peptides (as shown in Figure 4), although the viscoelasticity of RADA16-I was affected by the motifs of BMP7, the values of the storage modulus ($G'$) and loss modulus ($G''$) of the functionalized self-assembling peptides were similar to other RADA16-I-based functionalized peptide,[47] and even higher than other hydrogel biomaterial using in nucleus pulposus tissue engineering.[48] Nevertheless, like those of other hydrogels,[38,46,49] the mechanical properties of a single functionalized self-assembling peptide nanofibrous hydrogel are not very good. However, the RAD-SNV and RAD-KPS hydrogels significantly enhanced the secretion of aggrecan, which is the most important proteoglycan of the IVD. Therefore, as indicated in other reports,[50,51] we suggest that these functionalized self-assembling peptides are more suitable for patients with early stage IDD, such as Pfirrmann grade II or III, in which the AF and CE are mostly intact. However, whether the mechanical function of an IVD can be increased or restored will require further animal studies. In addition, the solubilized functionalized peptides rapidly self-assembled to form nanofibrous hydrogels under physiological conditions. This result indicated that these functionalized self-assembling peptides could be implanted into a disc via a minimally invasive injection, an approach which many studies have shown to be effective.[21,52,53] The results of this study indicated that the designed self-assembling peptides containing short BMP7 motifs have favorable feasibility for clinical applications in NP tissue engineering.

## 5. CONCLUSIONS

With an overall goal of repairing early-stage IDD, the specific aim of this study was to seek reliable biomaterials for NP tissue engineering. In the present study, we conjugated three different functional short peptides of BMP7 to the C-terminus of RADA16-I, and we mixed each one with RADA16-I to obtain functionalized self-assembling peptides. The results confirmed that all of the functionalized self-assembling peptide hydrogel scaffolds had excellent biocompatibilities for hdNPCs in vitro. The RAD-SNV and RAD-KPS scaffolds exhibited more promising bioactivities for hdNPCs than did the RAD-KAI scaffold in vitro, and the rates of aggrecan secretion and the expression of aggrecan and sox-9 mRNAs were significantly higher in hdNPCs grown in a RAD-KPS scaffold than in those in grown in a RAD-SNV scaffold. Notably, RAD-KPS showed good compatibility in vivo. Thus, the functionalized self-assembling peptides RAD-SNV and RAD-KPS show great potential for NP tissue-engineering applications, and RAD-KPS may have more potential than does RAD-SNV.

## AUTHOR INFORMATION


### Corresponding Authors

*E-mail: ruandikengh@163.com (D.R.).
*E-mail: wangdelinavy@163.com

### Author Contributions

⊥H.T., Y.W., and H.L. contributed equally to this work.


### Notes

The authors declare no competing financial interest.

## ACKNOWLEDGMENTS

We thank Dr. Liu Xi of Tsinghua University for her invaluable guidance in forming the hydrogels and Dr. Li Jie of the First Affiliated Hospital of Anhui Medical University for her excellent assistance in preparing the English edition of this manuscript.

## REFERENCES


(1) Rubin, D. I. Epidemiology and Risk Factors for Spine Pain. *Neurol Clin* **2007**, *25*, 353−371.

(2) Luo, X.; Pietrobon, R.; Sun, S. X.; Liu, G. G.; Hey, L. Estimates and Patterns of Direct Health Care Expenditures Among Individuals with Back Pain in the United States. *Spine (Philadelphia)* **2004**, *29*, 79−86.

(3) Luoma, K.; Riihimaki, H.; Luukkonen, R.; Raininko, R.; Viikari-Juntura, E.; Lamminen, A. Low Back Pain in Relation to Lumbar Disc Degeneration. *Spine (Philadelphia)* **2000**, *25*, 487−492.

(4) Pye, S. R.; Reid, D. M.; Smith, R.; Adams, J. E.; Nelson, K.; Silman, A. J.; O'Neill, T. W. Radiographic Features of Lumbar Disc Degeneration and Self-reported Back Pain. *J. Rheumatol.* **2004**, *31*, 753−758.

(5) Bydon, M.; De la Garza-Ramos, R.; Macki, M.; Baker, A.; Gokaslan, A. K.; Bydon, A. Lumbar Fusion versus Non-operative Management for Treatment of Discogenic Low Back Pain: A Systematic Review and Meta-analysis of Randomized Controlled Trials. *J. Spinal. Disord. Technol.* **2014**, *27*, 297−304.

(6) Sihawong, R.; Janwantanakul, P.; Jiamjarasrangsi, W. A Prospective, Cluster-randomized Controlled Trial of Exercise Program to Prevent Low Back Pain in Office Workers. *Eur. Spine. J.* . **2014**, *23*, 786−793.

(7) Bruehl, S.; Burns, J. W.; Gupta, R.; Buvanendran, A.; Chont, M.; Schuster, E.; France, C. R. Endogenous Opioid Inhibition of Chronic Low-back Pain Influences Degree of Back Pain Relief After Morphine Administration. *Reg. Anesth. Pain Med.* **2014**, *39*, 120−125.

(8) Gillet, P. The Fate of the Adjacent Motion Segments After Lumbar Fusion. *J. Spinal. Disord. Technol.* **2003**, *16*, 338−345.




DOI: 10.1021/acsami.5b03605
*ACS Appl. Mater. Interfaces* 2015, 7, 17076−17087

(9) Ruan, D.; He, Q.; Ding, Y.; Hou, L.; Li, J.; Luk, K. D. Intervertebral Disc Transplantation in the Treatment of Degenerative Spine Disease: A Preliminary Study. *Lancet* **2007**, *369*, 993−999.
(10) Schizas, C.; Kulik, G.; Kosmopoulos, V. Disc Degeneration: Current Surgical Options. *Eur. Cell Mater.* **2010**, *20*, 306−315.
(11) Colombier, P.; Clouet, J.; Hamel, O.; Lescaudron, L.; Guicheux, J. The Lumbar Intervertebral Disc: From Embryonic Development to Degeneration. *Jt., Bone, Spine* **2013**, *81*, 125−129.
(12) Adams, M. A.; Roughley, P. J. What is Intervertebral Disc Degeneration, and What Causes It? *Spine (Philadelphia)* **2006**, *31*, 2151−2161.
(13) Antoniou, J.; Steffen, T.; Nelson, F.; Winterbottom, N.; Hollander, A. P.; Poole, R. A.; Aebi, M.; Alini, M. The Human Lumbar Intervertebral Disc: Evidence for Changes in the Biosynthesis and Denaturation of the Extracellular Matrix with Growth, Maturation, Ageing, and Degeneration. *J. Clin. Invest.* **1996**, *98*, 996−1003.
(14) Hughes, S. P.; Freemont, A. J.; Hukins, D. W.; McGregor, A. H.; Roberts, S. The Pathogenesis of Degeneration of the Intervertebral Disc and Emerging Therapies in the Management of Back Pain. *J. Bone. Joint Surg. Br.* **2012**, *94-B*, 1298−1304.
(15) Fisher, M. B.; Mauck, R. L. Tissue engineering and regenerative medicine: recent innovations and the transition to translation. *Tissue Eng., Part B* **2013**, *19*, 1−13.
(16) Liang, C. Z.; Li, H.; Tao, Y. Q.; Peng, L. H.; Gao, J. Q.; Wu, J. J.; Li, F. C.; Hua, J. M.; Chen, Q. X. Dual Release of Dexamethasone and TGF-beta3 from Polymeric Microspheres for Stem Cell Matrix Accumulation in a Rat Disc Degeneration Model. *Acta Biomater.* **2013**, *9*, 9423−9433.
(17) Huh, H.; Lee, Y. J.; Kim, J. H.; Kong, M. H.; Song, K. Y.; Choi, G. The Effects of TWEAK, Fn14, and TGF-beta1 on Degeneration of Human Intervertebral Disc. *J. Korean Neurosurg. Soc.* **2010**, *47*, 30−35.
(18) Zhang, R.; Ruan, D.; Zhang, C. Effects of TGF-beta1 and IGF-1 on Proliferation of Human Nucleus Pulposus Cells in Medium with Different Serum Concentrations. *J. Orthop. Surg. Res.* **2006**, *1*, 9.
(19) Wang, H.; Zhou, Y.; Huang, B.; Liu, L. T.; Liu, M. H.; Wang, J.; Li, C. Q.; Zhang, Z. F.; Chu, T. W.; Xiong, C. J. Utilization of Stem Cells in Alginate for Nucleus Pulposus Tissue Engineering. *Tissue Eng., Part A* **2013**, *20*, 908−920.
(20) Chen, Y. C.; Su, W. Y.; Yang, S. H.; Gefen, A.; Lin, F. H. In Situ Forming Hydrogels Composed of Oxidized High Molecular Weight Hyaluronic Acid and Gelatin for Nucleus Pulposus Regeneration. *Acta Biomater.* **2013**, *9*, 5181−5193.
(21) Frith, J. E.; Cameron, A. R.; Menzies, D. J.; Ghosh, P.; Whitehead, D. L.; Gronthos, S.; Zannettino, A. C.; Cooper-White, J. J. An Injectable Hydrogel Incorporating Mesenchymal Precursor Cells and Pentosan Polysulphate for Intervertebral Disc Regeneration. *Biomaterials* **2013**, *34*, 9430−9440.
(22) Maude, S.; Ingham, E.; Aggeli, A. Biomimetic Self-assembling Peptides as Scaffolds for Soft Tissue Engineering. *Nanomedicine (London, U. K.)* **2013**, *8*, 823−847.
(23) Holmes, T. C.; de Lacalle, S.; Su, X.; Liu, G.; Rich, A.; Zhang, S. Extensive Neurite Outgrowth and Active Synapse Formation on Self-assembling Peptide Scaffolds. *Proc. Natl. Acad. Sci. U. S. A.* **2000**, *97*, 6728−6733.
(24) Kisiday, J.; Jin, M.; Kurz, B.; Hung, H.; Semino, C.; Zhang, S.; Grodzinsky, A. J. Self-assembling Peptide Hydrogel Fosters Chondrocyte Extracellular Matrix Production and Cell Division: Implications for Cartilage Tissue Repair. *Proc. Natl. Acad. Sci. U. S. A.* **2002**, *99*, 9996−10001.
(25) Doll, T. A.; Raman, S.; Dey, R.; Burkhard, P. Nanoscale Assemblies and Their Biomedical Applications. *J. R. Soc., Interface* **2013**, *10*, 20120740.
(26) Zhang, S.; Gelain, F.; Zhao, X. Designer Self-assembling Peptide Nanofiber Scaffolds for 3D Tissue Cell Cultures. *Semin. Cancer Biol.* **2005**, *15*, 413−420.
(27) Liu, X.; Wang, X.; Wang, X.; Ren, H.; He, J.; Qiao, L.; Cui, F. Z. Functionalized Self-assembling Peptide Nanofiber Hydrogels Mimic Stem Cell Niche to Control Human Adipose Stem Cell Behavior in Vitro. *Acta Biomater.* **2013**, *9*, 6798−6805.
(28) Horii, A.; Wang, X.; Gelain, F.; Zhang, S. Biological Designer Self-assembling Peptide Nanofiber Scaffolds Significantly Enhance Osteoblast Proliferation, Differentiation and 3-D Migration. *PLoS One* **2007**, *2*, e190.
(29) Gelain, F.; Bottai, D.; Vescovi, A.; Zhang, S. Designer Self-assembling Peptide Nanofiber Scaffolds for Adult Mouse Neural Stem Cell 3-dimensional Cultures. *PLoS One* **2006**, *1*, e119.
(30) Guo, H. D.; Cui, G. H.; Yang, J. J.; Wang, C.; Zhu, J.; Zhang, L. S.; Jiang, J.; Shao, S. J. Sustained Delivery of VEGF From Designer Self-Assembling Peptides Improves Cardiac Function After Myocardial Infarction. *Biochem. Biophys. Res. Commun.* **2012**, *424*, 105−111.
(31) An, H. S.; Takegami, K.; Kamada, H.; Nguyen, C. M.; Thonar, E. J.; Singh, K.; Andersson, G. B.; Masuda, K. Intradiscal Administration of Osteogenic Protein-1 Increases Intervertebral Disc Height and Proteoglycan Content in the Nucleus Pulposus in Normal Adolescent Rabbits. *Spine (Phila Pa 1976)* **2005**, *30* (25−31), 31−32.
(32) Chubinskaya, S.; Hurtig, M.; Rueger, D. C. OP-1/BMP-7 in Cartilage Repair. *Int. Orthop* **2007**, *31*, 773−781.
(33) Wang, C. F.; Zhang, C.; Wang, D. L.; Wu, J. H.; Zhang, Y.; Xu, C.; Xin, H. K.; He, Q.; Ruan, D. K. Nucleus Pulposus Cells Expressing hBMP7 Can Prevent the Degeneration of Allogenic IVD in a Canine Transplantation Model. *J. Orthop. Res.* **2013**, *31*, 1366−1373.
(34) Chen, Y.; Webster, T. J. Increased Osteoblast Functions in the Presence of BMP-7 Short Peptides for Nanostructured Biomaterial Applications. *J. Biomed. Mater. Res., Part A* **2009**, *91A*, 296−304.
(35) Tao, H.; Zhang, Y.; Wang, C. F.; Zhang, C.; Wang, X. M.; Wang, D. L.; Bai, X. D.; Wen, T. Y.; Xin, H. K.; Wu, J. H.; Liu, Y.; He, Q.; Ruan, D. Biological Evaluation of Human Degenerated Nucleus Pulposus Cells in Functionalized Self-Assembling Peptide Nanofiber Hydrogel Scaffold. *Tissue Eng., Part A* **2014**, *20*, 1621−31.
(36) Leung, V. Y.; Tam, V.; Chan, D.; Chan, B. P.; Cheung, K. M. Tissue Engineering for Intervertebral Disk Degeneration. *Orthop. Clin. North. Am.* **2011**, *42*, 575−583.
(37) Iatridis, J. C.; Nicoll, S. B.; Michalek, A. J.; Walter, B. A.; Gupta, M. S. Role of Biomechanics in Intervertebral Disc Degeneration and Regenerative Therapies: What Needs Repairing in the Disc and What Are Promising Biomaterials for Its Repair? *Spine J.* **2013**, *13*, 243−262.
(38) Koutsopoulos, S.; Zhang, S. Long-term Three-dimensional Neural Tissue Cultures in Functionalized Self-assembling Peptide Hydrogels, Matrigel and Collagen I. *Acta Biomater.* **2013**, *9*, 5162−5169.
(39) Liu, X.; Wang, X.; Horii, A.; Wang, X.; Qiao, L.; Zhang, S.; Cui, F. Z. In Vivo Studies on Angiogenic Activity of Two Designer Self-assembling Peptide Scaffold Hydrogels in the Chicken Embryo Chorioallantoic Membrane. *Nanoscale* **2012**, *4*, 2720−2727.
(40) Wang, C. F.; Ruan, D. K.; Zhang, C.; Wang, D. L.; Xin, H. K.; Zhang, Y. Effects of Adeno-associated Virus-2-mediated Human BMP-7 Gene Transfection on the Phenotype of Nucleus Pulposus Cells. *J. Orthop. Res.* **2011**, *29*, 838−845.
(41) Cheng, Y.; He, C.; Xiao, C.; Ding, J.; Cui, H.; Zhuang, X.; Chen, X. Versatile biofunctionalization of polypeptide-based thermosensitive hydrogels via click chemistry. *Biomacromolecules* **2013**, *14*, 468−475.
(42) Shim, W. S.; Kim, J. H.; Park, H.; Kim, K.; Chan, K. I.; Lee, D. S. Biodegradability and biocompatibility of a pH- and thermo-sensitive hydrogel formed from a sulfonamide-modified poly(epsilon-caprolactone-co-lactide)-poly(ethylene glycol)-poly(epsilon-caprolactone-co-lactide) block copolymer. *Biomaterials* **2006**, *27*, 5178−5185.
(43) Dolan, P.; Adams, M. A. Recent Advances in Lumbar Spinal Mechanics and Their Significance for Modelling. *Clin Biomech (Bristol, Avon)* **2001**, *16* (S), S8−S16.
(44) Antoniou, J.; Goudsouzian, N. M.; Heathfield, T. F.; Winterbottom, N.; Steffen, T.; Poole, A. R.; Aebi, M.; Alini, M. The Human Lumbar Endplate. Evidence of Changes in Biosynthesis and Denaturation of the Extracellular Matrix with Growth, Maturation, Aging, and Degeneration. *Spine (Philadelphia)* **1996**, *21*, 1153−1161.
(45) Roughley, P. J.; Alini, M.; Antoniou, J. The Role of Proteoglycans in Aging, Degeneration and Repair of the Intervertebral Disc. *Biochem. Soc. Trans.* **2002**, *30*, 869−874.
(46) Reitmaier, S.; Wolfram, U.; Ignatius, A.; Wilke, H. J.; Gloria, A.; Martin-Martinez, J. M.; Silva-Correia, J.; Miguel Oliveira, J.; Luís Reis,


DOI: 10.1021/acsami.5b03605
*ACS Appl. Mater. Interfaces* 2015, 7, 17076−17087

R.; Schmidt, H. Hydrogels for Nucleus Replacement–facing the Biomechanical Challenge. *J. Mech. Behav. Biomed. Mater.* **2012**, *14*, 67−77.
(47) Cheng, T. Y.; Chen, M. H.; Chang, W. H.; Huang, M. Y.; Wang, T. W. Neural Stem Cells Encapsulated in a Functionalized Self-assembling Peptide Hydrogel for Nrain Tissue Engineering. *Biomaterials* **2013**, *34*, 2005−2016.
(48) Tsaryk, R.; Gloria, A.; Russo, T.; Anspach, L.; De Santis, R.; Ghanaati, S.; Unger, R. E.; Ambrosio, L.; Kirkpatrick, C. J. Collagen-low Molecular Weight Hyaluronic Acid Semi-interpenetrating Network Loaded with Gelatin Microspheres for Cell and Growth Factor Delivery for Nucleus Pulposus Regeneration. *Acta Biomater.* **2015**, *20*, 10.
(49) Jeong, C. G.; Francisco, A. T.; Niu, Z.; Mancino, R. L.; Craig, S. L.; Setton, L. A. Screening of Hyaluronic Acid-poly(Ethylene Glycol) Composite Hydrogels to Support Intervertebral Disc Cell Biosynthesis Using Artificial Neural Network Analysis. *Acta Biomater.* **2014**, *10*, 3421−3430.
(50) Gawri, R.; Antoniou, J.; Ouellet, J.; Awwad, W.; Steffen, T.; Roughley, P.; Haglund, L.; Mwale, F. Best paper NASS 2013: link-N can stimulate proteoglycan synthesis in the degenerated human intervertebral discs. *Eur. Cell Mater.* **2013**, *02*, 107−119.
(51) Mercuri, J. J.; Patnaik, S.; Dion, G.; Gill, S. S.; Liao, J.; Simionescu, D. T. Regenerative Potential of Decellularized Porcine Nucleus Pulposus Hydrogel Scaffolds: Stem Cell Differentiation, Matrix Remodeling, and Biocompatibility Studies. *Tissue Eng., Part A* **2013**, *19*, 952−966.
(52) Orozco, L.; Soler, R.; Morera, C.; Alberca, M.; Sanchez, A.; Garcia-Sancho, J. Intervertebral disc repair by autologous mesenchymal bone marrow cells: a pilot study. *Transplantation* **2011**, *92*, 822−828.
(53) Balkovec, C.; Vernengo, J.; McGill, S. M. The use of a novel injectable hydrogel nucleus pulposus replacement in restoring the mechanical properties of cyclically fatigued porcine intervertebral discs. *J. Biomech. Eng.* **2013**, *135*, 061004−061005.


DOI: 10.1021/acsami.5b03605
*ACS Appl. Mater. Interfaces* 2015, 7, 17076−17087